Crespo-Hernández Carlos E. (Orcid ID: 0000-0002-3594-0890)

SPECIAL ISSUE RESEARCH ARTICLE

Author Manuscript

Electronic relaxation mechanism of 9-Methyl-2,6-Diaminopurine and 2,6-Diaminopurine-2'-Deoxyribose in solution†

Luis A. Ortiz-Rodríguez,[1,2] Naishka E. Caldero-Rodríguez,[1] Sourav Kanti Seth,[1] Karitza Díaz-González,[1] and Carlos E. Crespo-Hernández[1*]

1. *Department of Chemistry, Case Western Reserve University, Cleveland, OH 44106, USA.*
2. *Current address: Department of Chemistry, University of Michigan, Ann Arbor, Michigan 48104, USA*

* *Corresponding author e-mail:* carlos.crespo@case.edu (Carlos E. Crespo-Hernández)

†This article is part of a Special Issue dedicated to the topic of Nucleic Acid Photophysics

This is the author manuscript accepted for publication and has undergone full peer review but has not been through the copyediting, typesetting, pagination and proofreading process, which may lead to differences between this version and the Version of Record. Please cite this article as doi: 10.1111/php.13887

This article is protected by copyright. All rights reserved.

Author Manuscript

ABSTRACT

Prolonged ultraviolet exposure results in the formation of cyclobutane pyrimidine dimers (CPDs) in RNA. Consequently, prebiotic photolesion repair mechanisms should have played an important role in the maintenance of the structural integrity of primitive nucleic acids. 2,6-Diaminopurine (2,6DAP) is a prebiotic nucleobase that repairs CPDs with high efficiency when incorporated into polymers. We investigate the electronic deactivation pathways of 2,6-diaminopurine-2'-deoxyriside (2,6DAP-d) and 9-methyl-2,6-diaminopurine (9Me2,6DAP) in acetonitrile and aqueous solution to shed light on the photophysical and excited state properties of the 2,6-diaminopurine chromophore. Evidence is presented that both are photostable compounds exhibiting similar deactivation mechanisms upon population of the $S_1(\pi\pi^* L_a)$ state at 290 nm. The mechanism involves deactivation through two reaction coordinates (C2- and C6-coordinates) and >99% of the excited state population decays through non-radiative pathways involving two conical intersections with the ground state. The radiative and nonradiative lifetimes are longer in aqueous solution compared to acetonitrile. While τ_1 is similar in both derivatives, τ_2 is ca. 1.5-fold longer in 2,6-diaminopurine-2'-deoxyriside due to a more efficient trapping in the $S_1(\pi\pi^* L_a)$ minimum. Therefore, 2,6-diaminopurine could have accumulated in significant quantities during prebiotic times to be incorporated into non-canonical RNA and play a significant role in its photoprotection.

Author Manuscript

INTRODUCTION

The investigation of the electronic relaxation mechanisms and photostability/photoreactivity of nucleobases and their derivatives is essential for understanding the molecular origins of life.[1,2] As such, extensive research has been conducted over the years to explore the electronic relaxation pathways that are responsible for the inherent photostability of the pyrimidine and purine derivatives.[2–11] It has been shown that the photostability of these derivatives cannot be solely attributed to the pyrimidine and purine chromophores;[12,13] instead, the substituents present at the C2 and C4/C6 positions of the nucleobases play a crucial role at regulating their photostability when exposed to ultraviolet radiation (UVR).[14–22]

The genetic alphabet we witness today is a testament to the continuous refinement processes that have shaped prebiotic organic molecules on Earth. These evolutionary processes, constantly influenced by sunlight radiation, have underscored the utmost significance of photochemistry in the emergence of the current genetic code. Despite the established photostability of the nucleic acids, prolonged ultraviolet radiation exposure results in the photoinduced formation of adducts such as cyclobutane pyrimidine dimers (CPDs) and other photoproducts.[1,23,24] Mechanisms like photolyase-mediated repair and nucleotide excision repair (NER) can repair these photoadducts in modern organisms, however, they were not available during the prebiotic era when the first nucleic acid polymers and life forms emerged.[25–28] Therefore, prebiotic photolesion repair mechanisms should have played an important role in the maintenance of the structural integrity of primitive nucleic acids.

Recent studies have shown that the purine derivative 2,6-diaminopurine (2,6DAP) has the ability to repair CPDs through electron transfer with high efficiency when incorporated into nucleic acid strands due to its excellent electron-donating properties,[29] hinting at the possibility

Author Manuscript

that 2,6DAP may have been involved in RNA repair during the prebiotic period. The discovery that 2,6DAP could have been transported to Earth through meteorites like Murchison and LON94102 further emphasizes its potential significance during prebiotic times.[30] Additionally, the presence of 2,6DAP in other biological contexts, such as its replacement of adenine in the genome of phage S-2L of the cyanobacteria *Synechococcus elongatus*, further suggests its important role during the prebiotic era.[31–33]

In a recent study, the electronic relaxation mechanisms of 2,6DAP and 2,6-diaminopurine-2'-deoxyribose (2,6DAP-d) were investigated in aqueous solutions.[15] It was proposed that 2,6DAP could have accumulated in large enough quantities during the prebiotic era due to its high photostability.[15] Those results support the notion that 2,6DAP may have been involved in the formation of prebiotic oligomers, acting as photoprotective components for the prebiotic genetic code and potentially enhancing the photostability of higher-order nucleic acid structures.[29] In this contribution, we extend those investigations by studying the electronic deactivation pathways of 2,6DAP-d and 9-methyl-2,6-diaminopurine (9Me2,6DAP) in acetonitrile (MeCN) and in phosphate buffer solution at pH 7.4. 2,6DAP-d and 9Me2,6DAP were selected to block N7H and N9H tautomerization observed in 2,6DAP[15] and to investigate how the substitution of a methyl versus a 2'-deoxyribose at the N9 position affects the excited state dynamics of the 2,6DAP chromophore. Steady-state absorption and emission spectroscopies, femtosecond broadband transient absorption, and electronic-structure calculations are employed to elucidate their electronic deactivation mechanisms. In addition of aqueous solution, we have also chosen MeCN for investigation because it has been proposed that the polarity of this solvent (E_T(30)) more closely resemble the polarity experienced by the nucleobases when they are incorporated in nucleic acid strands than an aqueous environment.[34] Therefore, the effect of the solvent environment on the

photophysics and excited state relaxation pathways of both nucleobase derivatives is also investigated.

Author Manuscript

MATERIALS AND METHODS

Chemicals and steady-state measurements. 9-Methyl-9H-purine-2,6-diamine (9Me2,6DAP, 95% purity) and 2,6-diaminopurine-2'-deoxyribose (2,6DAP-d, 99% purity) were purchased from Enamine and Chem-Impex International, Inc. and were used as received. Acetonitrile (MeCN, HPLC grade) was purchased from Fisher Scientific.

A Cary 300 spectrophotometer and a Cary Eclipse spectrofluorimeter were used to measure the steady-state absorption and emission spectra, respectively. A scan rate of 120 nm/min and a PMT voltage of 600 V were used to record the emission spectra with 5 nm slit widths.

Phosphate buffer solutions were prepared with a concentration of 16 mM to ensure its precise performance. The composition of this buffer involved a balanced mixture containing 0.402 g of 10 mM monobasic potassium phosphate (KH_2PO_4) and 0.345 g of 6 mM dibasic potassium phosphate (K_2HPO_4). These salts were thoughtfully measured and dissolved in a total volume of 250 mL of ultra-pure water. To attain the desired pH of 7.4, a methodical approach was taken. A solution of 2 M sodium hydroxide (NaOH) was employed in conjunction with a precise pH meter. Gradual additions of the sodium hydroxide solution allowed for a controlled elevation of the pH to the target value of 7.4, ensuring the buffer's effectiveness for its intended application.

Author Manuscript

Electronic-structure calculations. ORCA 5.0 was used to perform all the quantum chemical calculations.[35] Ground- and excited state optimizations were performed using the B3LYP[36] functional and the cc-pVDZ basis set.[37] Minimum-energy crossing points between the lowest-energy singlet states were optimized using spin-flip time-dependent density functional theory (SF-TDDFT).[38,39] Implicitly solvent effects were modeled using the conductor-like polarizable continuum model (CPCM).[40] To increase the efficiency of the calculations, the RIJCOSX density fitting approximation was utilized.[41] Vertical excitation energies and potential energy profiles were calculated at the TD-BP86[42]/CPCM/def2-TZVPD[37]//B3LYP/CPCM/cc-pVDZ level of theory in MeCN. The magnitude of the oscillator strength and by visual inspection of the Kohn–Sham orbitals were used to determine the character of the excited states.

Femtosecond broadband transient absorption spectroscopy. The excited state relaxation mechanisms of 9Me2,6DAP and 2,6DAP-d in MeCN and phosphate buffer at pH 7.4 were studied using broadband transient absorption spectroscopy. The experimental setup has been discussed in detail elsewhere.[43] Briefly, a 1 kHz, 100 fs laser pulse at 800 nm was generated using a regenerative amplifier (Coherent Libra-HE), which is seeded with a Ti:Sapphire oscillator (Vitesse, Coherent). An optical parametric amplifier (TOPAS, Quantronix/Light Conversion) was used to generate the excitation wavelength at 290 nm and the white light continuum from 320 to 700 nm was generated with a continuously moving 2 mm calcium fluoride (CaF_2) crystal. Fresh solutions were used under continuous stirring in fused silica cells with a 2 mm path length to guarantee sample homogeneity and that a fresh sample volume was always excited. Absorption spectroscopy was used to monitor the possibility of photodegradation during laser experiments. The samples were replaced with fresh solutions if the absorbance maximum of the lowest energy absorption band decreased by more

than 3%. Global and target analyses of the transient absorption data were performed using the Glotaran graphical user interface to the R-package TIMP software.[44]

Author Manuscript

RESULTS

Steady-state photophysics

9Me2,6DAP and 2,6DAP-d consists of the purine nucleobase substituted with two amino groups at the C2 and C6 positions and a methyl group and a 2'-deoxyribose at the N9 position for 9Me2,6DAP and 2,6DAP-d, respectively (Scheme 1). The substitution at the N9 position effectively prevents N9H and N7H tautomerization, resulting in the biologically relevant single tautomer for both derivatives. The steady-state photophysical properties collected in this study for 9Me2,6DAP and 2,6DAP-d are summarized in Table 1. In Figure 1, the molar absorption spectra of 9Me2,6DAP and 2,6DAP-d in MeCN and phosphate buffer at pH 7.4 are depicted. Notably, both compounds display three distinct absorption bands around 280, 256, and 215 nm. In MeCN, 2,6DAP-d has molar absorption coefficients of $(9.1 \pm 0.1) \times 10^3$ M^{-1} cm^{-1} at 280 nm, $(8.2 \pm 0.1) \times 10^3$ M^{-1} cm^{-1} at 256 nm and $(2.4 \pm 0.1) \times 10^4$ M^{-1} cm^{-1} at 217 nm. For 9Me2,6DAP in phosphate buffer at pH 7.4, molar absorption coefficients at the absorption maxima of $(9.5 \pm 0.1) \times 10^3$ M^{-1} cm^{-1} at 280 nm, $(7.4 \pm 0.1) \times 10^3$ M^{-1} cm^{-1} at 257 nm, and $(2.6 \pm 0.1) \times 10^4$ M^{-1} cm^{-1} at 215 nm were measured. For 9Me2,6DAP in MeCN, molar absorption coefficients at the absorption maxima of $(9.4 \pm 0.1) \times 10^3$ M^{-1} cm^{-1} at 280 nm, $(8.0 \pm 0.1) \times 10^3$ M^{-1} cm^{-1} at 257 nm, and $(2.8 \pm 0.1) \times 10^4$ M^{-1} cm^{-1} at 217 nm were measured. The replacement of 9N-methyl group for 2'-deoxyribose induces a minor hyperchromic effect in the absorption spectrum, and the molar

absorption coefficients slightly change to $(9.6 \pm 0.1) \times 10^3$ M^{-1} cm^{-1} at 280 nm, $(8.6 \pm 0.1) \times 10^3$ M^{-1} cm^{-1} at 256 nm and $(2.3 \pm 0.1) \times 10^4$ M^{-1} cm^{-1} at 215 nm in phosphate buffer solutions.

<Scheme 1>

<Figure 1>

<Table 1>

The emission spectra of 9Me2,6DAP and 2,6DAP-d in MeCN are also shown in Figure 1a. The excitation spectrum collected at the 330 nm emission wavelength satisfactorily match the absorption spectrum of 9Me2,6DAP in MeCN (Figure S1). This evidence that the fluorescence emission is an intrinsic property of 9Me2,6DAP. The emission spectra of both 9Me2,6DAP and 2,6DAP-d exhibit maxima at 335 ± 2 nm. The fluorescence quantum yields of 9Me2,6DAP and 2,6DAP-d in MeCN were determined to be practically similar upon excitation at 290 nm, 0.0020 ± 0.0001 and 0.0025 ± 0.0001, respectively, using tryptophan as a standard.[45] In addition, a 0-0 energy of the lowest-energy excited singlet state of 4.13 eV was estimated for both molecules from the crossing point between the absorption and emission spectra in MeCN (Figure 1). Figure 1b shows the emission spectra of 9Me2,6DAP and 2,6DAP-d recorded in phosphate buffer at pH 7.4. The emission spectra of both 9Me2,6DAP and 2,6DAP-d exhibit maxima at 352 ± 2 nm or a 17 nm redshift compared to the MeCN solutions. The fluorescence quantum yields were determined in phosphate buffer upon excitation at 290 nm to be 0.0042 ± 0.0001 for 9Me2,6DAP and 0.0058 ± 0.0008 for 2,6DAP-d, respectively, also using tryptophan as a standard.[45] A *0-0* energy of the lowest-energy excited singlet state of 4.09 eV was estimated for both molecules from the crossing point between the absorption and emission spectra in phosphate buffer (Figure 1b).

Electronic-structure calculations of 9Me2,6DAP

Author Manuscript

Author Manuscript

The ground-state geometry of 9Me2,6DAP at the B3LYP/CPCM/cc-pVDZ level of theory in MeCN is mostly planar with only the hydrogen atoms of the amino group out of the molecular plane of the purine chromophore (Figure 2a). Vertical excitation energies were used to characterize the excited states available for deactivation upon excitation with 290 nm. Upon excitation with 290 nm (4.3 eV), the lowest-energy excited singlet state is populated. As shown in Table 2 and Figure 2b, this state has ππ* character (f = 0.17) and is dominated by a main (0.82) HOMO → LUMO electronic transition. Hence, from this point forward, we will refer to this state as S_1(ππ* L_a), using the nomenclature of Platt-Murell,[46] where the L_a label represents the state with the highest contribution of the HOMO → LUMO single electron transition. The calculated vertical energy for the S_1(ππ* L_a) in acetonitrile is in good agreement with the experimental value reported in Table 1, further supporting the appropriateness of the level of theory used in this study. The vertical excitation energies reported in Table 2 for 9Me2,6DAP are also in line with those reported previously for the N9H tautomer of 2,6DAP in water.[15] Below the S_1(ππ* L_a), there are two excited triplet states of ππ* character with energies of 3.34 and 4.13 eV in MeCN. Because the triplet states are also of ππ* character, intersystem crossing from the S_1(ππ* L_a) to these two triplet states is not expected to be favorable according to El-Sayed propensity rules.[47,48]

<FIGURE 2>

<Table 2>

The S_1(ππ* L_a) excited state minimum was also optimized at the TD-B3LYP/CPCM/cc-pVDZ level of theory in MeCN. At this level of theory, the minimum is mostly planar with only the hydrogen atoms of the amino group out of the molecular plane of the purine chromophore (Figure 2a) and is 3.96 eV adiabatically from the ground-state. In addition, two S_1(ππ* L_a)/S_0

Author Manuscript

minimum-energy crossing points or conical intersections were located, which are labeled as C6-CI and C2-CI in Figure 2a. The optimization of these minimum-energy crossing points was done using SF-TDDFT instead of LR-TDDFT, because LR-TDDFT cannot correctly describe the dimensionality of conical intersections (CI) between excited states and the ground-state.[49] The SF approach has been used extensively to overcome the problem with the conical intersections between the ground and excited states,[38,39,50] and it has been shown to provide the correct dimensionality of the CIs.[51,52] Furthermore, we note that the conical intersections identified in this work are similar to those reported by Szabla et al.,[29] and Oliveira et al.,[53] at the ADC(2) and MS-CASPT2 level of theories, respectively, providing additional support for the use of SF-TD-DFT in this study.

As shown in Figure 2, the C6-CI is characterized by significant out-of-plane distortion on the C6 atom and complete out of the molecular plane displacement of the amino group attached to this atom. Similarly, the C2-CI is characterized by significant out-of-plane distortion of the amino group on the C2 atom. To gather a general understanding of the topology of the state potential energy surface and to investigate the accessibility to the minimum-energy crossing points, we also performed optimizations along the N6C6C5C4 and N2C2N3C4 dihedral angles coordinates (a.k.a., relaxed surface scans) to capture the transition from the mostly planar structure of the excited state minimum to the C6-CI and C2-CI, respectively. Figure 3 shows the potential energy profiles constructed along the C6- and C2-puckering coordinates for 9Me2,6DAP at the TD-BP86/CPCM/def2-TZVP//TD-B3LYP/CPCM/cc-pVDZ level of theory in MeCN. On the one hand, the C6-CI can be accessed by surmounting a small energy barrier of 0.08 eV. On the other hand, the population that reaches the $S_1(\pi\pi^*\ L_a)$ minimum needs to overcome an energy barrier of 0.35 eV to access the C2-CI. Similar energy barriers of 0.4 eV to access the C2-CI and of 0.05 eV

to access the C6-CI were obtained for the N9H tautomer of 2,6DAP in water at the TD-BP86/CPCM/def2-TZVP//TD-B3LYP/CPCM/cc-pVDZ level of theory.[15] In vacuum, Oliveira et al.[53] reported upper-limit energy barriers of 0.83 and 0.57 eV to access the C2-CI and C6-CI from the $S_1(\pi\pi^*\ L_a)$ minimum at the MS(3)-CASPT2(14,11)/cc-pVDZ level of theory, which are in qualitative agreement with those reported in this study in MeCN. Therefore, the calculations predict that the $S_1(\pi\pi^*\ L_a)$ state population should decay significantly faster to the ground state through the C6-coordinate than through the C2-coordinate both in solution and in the gas phase.

<Figure 3>

Femtosecond broadband transient absorption measurements in MeCN

Femtosecond transient absorption measurements covering a spectral range from 350 to 700 nm, and a temporal window of up to 3 ns, were performed to elucidate the electronic deactivation pathways of 9Me2,6DAP and 2,6DAP-d in MeCN upon 290 nm excitation. Contour plots, representative decay traces with best kinetic fits, and the two-dimensional transient absorption spectral for 9Me2,6DAP and 2,6DAP-d are reported in Figures 4 and 5, respectively. Upon 290 nm excitation, three transient absorption bands are observed within the cross-correlation of the pump and probe beams in both molecules. These bands are centered at 651, 482 and 387 nm for 9Me2,6DAP and at 652, 488 and 385 nm for 2,6DAP-d. After reaching their maximum amplitude, all three transient absorption bands decay monotonically within 90 ps time delays. Lifetimes obtained from global and target analyses using a two-component or two exponential sequential kinetic model are reported in Table 3. As shown in Table 3, τ_1 has the same magnitude in 9Me2,6DAP than in 2,6DAP-d, while τ_2 is 1.5-fold longer in 2,6DAP-d than in 9Me2,6DAP. The evolution-associated difference spectra corresponding to the extracted lifetimes in MeCN are reported in Figures S2 and S3 for 9Me2,6DAP and 2,6DAP-d, respectively.

Author Manuscript

Author Manuscript

<Figure 4>

<Table 3>

<Figure 5>

Femtosecond broadband transient absorption measurements in phosphate buffer at pH 7.4

Transient absorption experiments for 9Me2,6DAP and 2,6DAP-d were also performed in aqueous phosphate buffer solutions at pH 7.4 upon 290 nm excitation. Contour plots, representative decay traces with best kinetic fits, and the two-dimensional transient absorption spectral for 9Me2,6DAP and 2,6DAP-d are reported in Figures 6 and 7, respectively. Similar to the transient spectra in MeCN, three transient absorption bands are observed within the cross-correlation of the pump and probe beams in both molecules. The transient bands for 9Me2,6DAP and 2,6DAP-d in aqueous phosphate buffer exhibit different relative amplitude and are slightly blue shifted compared to those in MeCN. After reaching their maximum amplitude, all three transient absorption bands decay monotonically within ca. 300 ps time delays. Lifetimes obtained from global and target analyses using a two-component sequential or two exponential kinetic model are reported in Table 3. As shown in Table 3, τ_1 has the same magnitude in 9Me2,6DAP than in 2,6DAP-d, while τ_2 is 1.4-fold longer in 2,6DAP-d than in 9Me2,6DAP. The evolution-associated difference spectra corresponding to the extracted lifetimes in MeCN are reported in Figures S4 and S5 for 9Me2,6DAP and 2,6DAP-d, respectively.

<Figure 6>

<Figure 7>

DISCUSSION

Author Manuscript

Proposed electronic relaxation mechanism for 9Me2,6DAP and 2,6DAP-d in MeCN

Considering the similarities in the steady-state properties reported in Figure 1 and the transient absorption spectra reported in Figures 4 to 7, the general electronic relaxation mechanism for both 9Me2,6DAP and 2,6DAP-d in MeCN and in phosphate buffer at pH 7.4 should be the same. As reported in "Electronic-structure calculations of 9Me2,6DAP", excitation of 9Me2,6DAP at 290 nm results in population of the $S_1(\pi\pi^*\ L_a)$ state. Hence, we assign the first lifetime to a competitive process in the $S_1(\pi\pi^*\ L_a)$ potential energy surface, where a fraction of the excited state population internally converts to the ground state through the near-barrierless C6-CI and another fraction populates the $S_1(\pi\pi^*\ L_a)$ minimum (see, Figure 3). The second lifetime is assigned to fluorescence emission from the $S_1(\pi\pi^*\ L_a)$ minimum and the simultaneous internal conversion to the ground state after surmounting the C2-CI. These assignments are supported by the observation that the EADS associated to the first lifetime can be assigned to a linear combination of the excited state absorption of the $S_1(\pi\pi^*\ L_a)$ minimum and the absorption spectrum of C6-CI, while the EADS associated to the second lifetime can be assigned to a linear combination with equal contribution of the individual $S_1(\pi\pi^*\ L_a)$ minimum and C2-CI excited absorption spectra (Figure S2). We remark, however, that the spectra of both CIs and the EADSs are very similar. In agreement with the vertical excitations energies reported in Table 2 in "Electronic-structure calculations of 9Me2,6DAP", and with the El-Sayed selection rules, population of longer-lived singlet or triplet states with $n\pi^*$ or $\pi\pi^*$ character is not observed.

In a recent investigation, the excited state dynamics of 2,6DAP and 2,6DAP-d were examined in aqueous solution.[15] It was proposed that the excited state population in the Franck-Condon region of the $S_1(\pi\pi^*\ L_a)$ state also branches in ultrafast timescales via the C2- and C6-puckering relaxation coordinates following excitation at 287 nm.[15] Herein, we have also identified

Author Manuscript

both coordinates for 9Me2,6DAP-d. On the one hand, we propose that in 9Me2,6DAP and 2,6DAP-d, the population following the C6-coordinate internally converts to the ground state in an ultrafast fashion considering the small energy barrier (<0.1 eV) associated with the C6-CI. On the other hand, we propose that the fraction of the population that branches into the C2-coordinates decays by a combination of internal conversion through the C2-CI and radiative decay due to the associated larger energy barrier (0.35 eV) to access the C2-CI. Therefore, as recently shown for 2,6DAP and 2,6DAP-d in aqueous solution,[15] we propose that τ_1 corresponds to a competition of the excited state population in the Franck-Condon region to either internally convert to the ground-state through the C6-CI or to populate the $S_1(\pi\pi^*\ L_a)$ minimum in the C2-coordinate. We assign τ_2 to simultaneous internal conversion through C2-CI and fluorescence emission (~0.60 to 0.20%) from the $S_1(\pi\pi^*\ L_a)$ minimum. This electronic relaxation mechanism is also supported by the transient absorption data reported in Figures 6 and 7 for 9Me2,6DAP and 2,6DAP-d in aqueous phosphate solution at pH 7.4. Therefore, the deactivation of the $S_1(\pi\pi^*\ L_a)$ population in both 9Me2,6DAP and 2,6DAP-d is driven by a combination of non-radiative and radiative internal conversion decay pathways to the ground state, resulting in the high photostability for both 2,6DAP derivatives in both MeCN and phosphate buffer solution. The proposed electronic relaxation mechanism is presented in Scheme 2.

<Scheme 2>

Role of the solvent on the excited state dynamics of 2,6DAP

The fluorescence data and transient absorption lifetimes obtained in back-to-back experiments for 9Me2,6DAP and 2,6DAP-d in MeCN and in phosphate buffer at pH 7.4 evidence that the $S_1(\pi\pi^*\ L_a)$ minimum is stabilized in aqueous solution compared to MeCN. For both 9Me2,6DAP and 2,6DAP-d, the fluorescence maximum redshifts by 17 nm, while the fluorescence quantum yield

and τ_2 increase in phosphate buffer compared with MeCN by 1.2 to 1.3-fold and 1.4 to 1.5-fold, respectively. The increase in τ_2 in going from MeCN to phosphate buffer suggests that a larger energy barrier needs to be surmounted to access the C2-CI in both 9Me2,6DAP and 2,6DAP-d in phosphate buffer. Similarly, a larger energy barrier needs to be surmounted to access the C6-CI in phosphate buffer relative to in MeCN for both molecules.

We note that the τ_1 and τ_2 for 9Me2,6DAP and 2,6DAP-d are 2.2- and 2.7-fold and 2.2- and 2.5-fold, respectively, longer in aqueous solution than in MeCN. We propose that one factor that could be contributing to the longer lifetimes when going from MeCN to aqueous solution is the 3-fold higher viscosity of water relative to MeCN, which can slow down the dynamics by hindering the out-of-plane nuclear relaxation process to access the C2 and C6 CIs. This can be also supported by the 2.1- and 2.3-fold higher fluorescence quantum yield obtained for 9Me2,6DAP and 2,6DAP-d in aqueous solution relative to MeCN (Figure S1). Yet, another factor that could explain the observed solvent effects is explicit solute-solvent hydrogen bonding interactions in aqueous solution that may also slowdown the dynamics relative to in acetonitrile. Therefore, in general, the radiative and nonradiative lifetimes for both 9Me2,6DAP and 2,6DAP-d slowdown in phosphate buffer compared to MeCN, but the magnitudes are still long enough (i.e., tens of picoseconds) to allow the photorepair of CPDs when incorporated in prebiotic RNA oligomers.[29]

Role of the N9 substituent on the excited state dynamics of 2,6DAP

The fluorescence quantum yields and transient absorption lifetimes obtained in back-to-back experiments for 9Me2,6DAP and 2,6DAP-d in MeCN and in phosphate buffer at pH 7.4 evidence that the substituent in the N9 position has a significant effect in the excited state dynamics of 2,6DAP. While the first lifetime for both 9Me2,6DAP and 2,6DAP-d has the same magnitude on

Author Manuscript

each solvent, the second lifetime is 1.4 and 1.5-fold longer for 2,6DAP-d compared to that of 9Me2,6DAP in phosphate buffer and MeCN, respectively. A small energy barrier in the $S_1(\pi\pi^*\ L_a)$ potential energy surface to access the C6-CI with the ground state can explain the similar τ_1 observed in both molecules. The longer τ_2 observed for 2,6DAP-d compared to that of 9Me2,6DAP can be explained by a more efficient trapping of the $S_1(\pi\pi^*\ L_a)$ population in its minimum before it can decay radiatively or nonradiatively through the C2-CI to the ground state. This is supported by the observation that the fluorescence quantum yields of 2,6DAP-d are ca. 1.4 and 1.3-fold larger than those of 9Me2,6DAP in phosphate buffer and MeCN, respectively. The more efficient trapping of the population in the $S_1(\pi\pi^*\ L_a)$ minimum of 2,6DAP-d could be due to an increase in the energy barrier to access the C2-CI. It could also be due to the more efficient relaxation of the excess vibrational energy in the $S_1(\pi\pi^*\ L_a)$ state in 2,6DAP-d compared to 9Me2,6DAP given the additional degrees of vibrational freedom imparted by the 2'-deoxyribose at the N9 position compared to the methyl group. The presence of a 2'-deoxyribose substituent introduces additional degrees of freedom compared to the methyl group, which allows the excess of vibrational energy in the $S_1(\pi\pi^*\ L_a)$ state to dissipate more efficiently. This in turns could trap the population in the $S_1(\pi\pi^*\ L_a)$ minimum more efficiently and slow down internal conversion to the ground state through the C2-CI or fluorescence emission. Intramolecular hydrogen bonding between the 2'-deoxyribose and the 2,6DAP nucleobase could also be another factor affecting this lifetime in 2,6DAP-d compared to 9Me2,6DAP. Importantly, the longer τ_2 lifetime of 2,6DAP-d in both phosphate buffer and MeCN is expected to increase the probability of photorepair of CPDs when incorporated in prebiotic RNA oligomers.[29]

CONCLUSION

Author Manuscript

Author Manuscript

The photophysics, electronic structure, and excited state dynamics of the prebiotic candidates 9Me2,6DAP and 2,6DAP-d have been investigated in MeCN and in phosphate buffer at pH 7.4. It is demonstrated that both 9Me2,6DAP and 2,6DAP-d are photostable compounds that exhibit nearly identical electronic relaxation mechanisms upon population of the $S_1(\pi\pi^* L_a)$ state at 290 nm. The electronic relaxation mechanism involves the competitive nonradiative deactivation of >99% of the population through two conical intersections and less than 1% fluorescence emission from the $S_1(\pi\pi^* L_a)$ minimum. The CIs are characterized by significant out-of-plane distortion of the C2 and C6 atoms and complete out of the molecular plane displacement of the corresponding amino groups. Relaxation of the $S_1(\pi\pi^* L_a)$ population through the C6-CI to the ground state has a very small energy barrier of ca. 0.05 to 0.08 eV in solution, while relaxation through the C2-CI to the ground state requires the surmounting of an energy barrier of ca. 0.4 eV. Both the solvent and the functional group at the N9 position modulate relaxation through the C2-coordinate, with both 2'-deoxyribose and aqueous solution increasing the τ_2 lifetime relative to MeCN and 9-methyl, respectively. Collectively, the experimental and computational results presented in this study and elsewhere[15] support the idea that the 2,6DAP chromophore should have accumulated in significant quantities during prebiotic times to participate in the formation of non-canonical RNA and play a significant role in the photorepair of CPDs in prebiotic RNA oligonucleotides.[29]

ACKNOWLEDGMENTS

Funding from the National Science Foundation (Grant No. CHE-1800052) is acknowledged. The authors also acknowledge the High-Performance Computing Resource in the Core Facility for Advanced Research Computing at Case Western Reserve University.

Author Manuscript

SUPPORTING INFORMATION

Additional supporting information may be found online in the Supporting Information section at the end of the article:

AUTHORS CONTRIBUTIONS

Luis A. Ortiz-Rodríguez: investigation, formal analysis, writing-original draft, writing review and editing.

Naishka E. Caldero-Rodríguez: investigation and formal analysis.

Sourav Kanti Seth: investigation and formal analysis.

Karitza Díaz-González: investigation and formal analysis.

Carlos E. Crespo-Hernández: conceptualization, funding acquisition, project administration, resources, supervision, visualization, validation, writing review and editing.

NOTE

The authors declare no conflicts of interest.

REFERENCES

1 S. J. Hoehn, N. E. Caldero-Rodríguez, C. E. Crespo-Hernández, "Photochemistry of RNA, RNA Monomers, and Plausible Prebiotic Precursors" In DNA Photodamage: From Light Absorption to Cellular Responses and Skin Cancer; edited by T. Douki, R. Improta, (Invited Review Chapter), *Photochem. Photobiol. Sci.*, 2022, Chapter 9, 197-226.

2 A. A. Beckstead, Y. Zhang, M. S. de Vries and B. Kohler, Life in the light: nucleic acid photoproperties as a legacy of chemical evolution, *Phys. Chem. Chem. Phys.*, 2016, **18**, 24228–24238.

Author Manuscript

3 W. J. Schreier, P. Gilch and W. Zinth, Early events of DNA photodamage, *Annu. Rev. Phys. Chem.*, 2015, **66**, 497–519.

4 C. T. Middleton, K. de La Harpe, C. Su, Y. K. Law, C. E. Crespo-Hernández and B. Kohler, DNA excited-state dynamics: from single bases to the double helix, *Annu. Rev. Phys. Chem.*, 2009, **60**, 217–239.

5 K. Kleinermanns, D. Nachtigallová and M. S. de Vries, Excited state dynamics of DNA bases, *Int. Rev. Phys. Chem.*, 2013, **32**, 308–342.

6 M. S. de Vries and P. Hobza, Gas-phase spectroscopy of biomolecular building blocks, *Annu. Rev. Phys. Chem.*, 2007, **58**, 585–612.

7 L. Serrano-Andres and M. Merchan, Are the five natural DNA/RNA base monomers a good choice from natural selection?: A photochemical perspective, *J. Photochem. Photobiol. C Photochem. Rev.*, 2009, **10**, 21–32.

8 P. R. Callis, Electronic states and luminescence of nucleic acid systems, *Annu. Rev. Phys. Chem.*, 1983, **34**, 329–357.

9 V. G. Stavros and J. R. R. Verlet, Gas-phase femtosecond particle spectroscopy: a bottom-up approach to nucleotide dynamics, *Annu. Rev. Phys. Chem.*, 2016, **67**, 211–232.

10 M. Pollum, M., L. Martínez-Fernández and C. E. Crespo-Hernández "Photochemistry of nucleic acid bases and their thio- and aza-analogues in solution. In Photoinduced Phenomena in NucleicAcids I", Vol.355; edited by M. B. Barbatti, A. C. Borin and S. Ulrich, 2015, 245–327.

11 C. E. Crespo-Hernández, B. Cohen, P. M. Hare and B. Kohler, Ultrafast excited-state

Author Manuscript

dynamics in nucleic acids, *Chem. Rev.*, 2004, **104**, 1977–2019.

12 C. E. Crespo-Hernández, L. Martínez-Fernández, C. Rauer, C. Reichardt, S. Mai, M. Pollum, P. Marquetand, L. González and I. Corral, Electronic and structural elements that regulate the excited-state dynamics in purine nucleobase derivatives, *J. Am. Chem. Soc.*, 2015, **137**, 4368–4381.

13 E. M. Arpa, M. M. Brister, S. J. Hoehn, C. E. Crespo-Hernández and I. Corral, On the Origin of the Photostability of DNA and RNA Monomers: Excited State Relaxation Mechanism of the Pyrimidine Chromophore, *J. Phys. Chem. Lett.*, 2020, **11**, 5156–5161.

14 E. Vos, S. J. Hoehn, S. E. Krul, C. E. Crespo-Hernández, J. González-Vázquez and I. Corral, Disclosing the Role of C4-Oxo Substitution in the Photochemistry of DNA and RNA Pyrimidine Monomers: Formation of Photoproducts from the Vibrationally Excited Ground State, *J. Phys. Chem. Lett.*, 2022, **13**, 2000–2006.

15 N. E. Caldero-Rodríguez, L. A. Ortiz-Rodríguez, A. A. Gonzalez and C. E. Crespo-Hernández, Photostability of 2, 6-diaminopurine and its 2′-deoxyriboside investigated by femtosecond transient absorption spectroscopy, *Phys. Chem. Chem. Phys.* 2022, 24, 4024–4211.

16 N. E. Caldero-Rodríguez and C. E. Crespo-Hernández, Excited state dynamics of 2′-deoxyisoguanosine and isoguanosine in aqueous solution, *Phys. Chem. Chem. Phys.*, 2022, **24**, 6769–6781.

17 N. E. Caldero-Rodríguez, E. M. Arpa, D. J. Cárdenas, L. Martínez-Fernández, S. Jockusch, S. K. Seth, I. Corral and C. E. Crespo-Hernández, 2-Oxopurine Riboside: A Dual Fluorescent Analog and Photosensitizer for RNA/DNA Research, *J. Phys. Chem. B*,

Author Manuscript

2022, **126**, 4483–4490.

18 S. J. Hoehn, S. E. Krul, B. J. Skory and C. E. Crespo-Hernández, Increased Photostability of the Integral mRNA Vaccine Component N1-Methylpseudouridine Compared to Uridine, *Chem. Eur. J.*, 2022, **28**, e202103667.

19 S. E. Krul, S. J. Hoehn, K. J. Feierabend and C. E. Crespo-Hernández, Excited state dynamics of 7-deazaguanosine and guanosine 5′-monophosphate, *J. Chem. Phys.*, 2021, **154**, 75103.

20 L. Martínez-Fernández, S. Arslancan, D. Ivashchenko, C. E. Crespo-Hernández and I. Corral, Tracking the origin of photostability in purine nucleobases: the photophysics of 2-oxopurine, *Phys. Chem. Chem. Phys.*, 2019, **21**, 13467–13473.

21 M. M. Brister and C. E. Crespo-Hernández, Excited-state dynamics in the RNA nucleotide uridine 5'-Monophosphate investigated using femtosecond broadband transient absorption spectroscopy, *J. Phys. Chem. Lett.*, 2019, **10**, 2156–2161.

22 M. M. Brister, M. Pollum and C. E. Crespo-Hernández, Photochemical etiology of promising ancestors of the RNA nucleobases (vol 18, pg 20097, 2016), *Phys. Chem. Chem. Phys.*, 2016, **18**, 22731.

23 S. Mouret, C. Baudouin, M. Charveron, A. Favier, J. Cadet and T. Douki, Cyclobutane pyrimidine dimers are predominant DNA lesions in whole human skin exposed to UVA radiation, *Proc. Natl. Acad. Sci.*, 2006, **103**, 13765–13770.

24 W. J. Schreier, T. E. Schrader, F. O. Koller, P. Gilch, C. E. Crespo-Hernández, V. N. Swaminathan, T. Carell, W. Zinth and B. Kohler, Thymine dimerization in DNA is an

Author Manuscript

ultrafast photoreaction, *Science*, 2007, **315**, 625–629.

25 C. Tan, Z. Liu, J. Li, X. Guo, L. Wang, A. Sancar and D. Zhong, The molecular origin of high DNA-repair efficiency by photolyase, *Nat. Commun.*, 2015, **6**, 1–6.

26 A. Mees, T. Klar, P. Gnau, U. Hennecke, A. P. M. Eker, T. Carell and L.-O. Essen, Crystal structure of a photolyase bound to a CPD-like DNA lesion after in situ repair, *Science*, 2004, **306**, 1789–1793.

27 W. L. de Laat, N. G. J. Jaspers and J. H. J. Hoeijmakers, Molecular mechanism of nucleotide excision repair, *Genes & Dev.*, 1999, **13**, 768–785.

28 J. O. Fuss and P. K. Cooper, DNA repair: dynamic defenders against cancer and aging, *PLoS Biol.*, 2006, **4**, e203.

29 R. Szabla, M. Zdrowowicz, P. Spisz, N. J. Green, P. Stadlbauer, H. Kruse, J. Šponer and J. Rak, 2, 6-diaminopurine promotes repair of DNA lesions under prebiotic conditions, *Nat. Commun.*, 2021, **12**, 1–11.

30 M. P. Callahan, K. E. Smith, H. J. Cleaves, J. Ruzicka, J. C. Stern, D. P. Glavin, C. H. House and J. P. Dworkin, Carbonaceous meteorites contain a wide range of extraterrestrial nucleobases, *Proc. Nat. Acad. Sci. U. S. A.*, 2011, **108**, 13995–13998.

31 Y. Zhou, X. Xu, Y. Wei, Y. Cheng, Y. Guo, I. Khudyakov, F. Liu, P. He, Z. Song, Z. Li and others, A widespread pathway for substitution of adenine by diaminopurine in phage genomes, *Science*, 2021, **372**, 512–516.

32 I. Y. Khudyakov, M. D. Kirnos, N. I. Alexandrushkina and B. F. Vanyushin, Cyanophage S-2L contains DNA with 2, 6-diaminopurine substituted for adenine, *Virology*, 1978, **88**,

Author Manuscript

8–18.

33 M. D. Kirnos, I. Y. Khudyakov, N. I. Alexandrushkina and B. F. Vanyushin, 2-Aminoadenine is an adenine substituting for a base in S-2L cyanophage DNA, *Nature*, 1977, **270**, 369–370.

34 C. Reichardt, Polarity of ionic liquids determined empirically by means of solvatochromic pyridinium N-phenolate betaine dyes, *Green Chem.*, 2005, **7**, 339–351.

35 F. Neese, F. Wennmohs, U. Becker and C. Riplinger, The ORCA quantum chemistry program package, *J. Chem. Phys.*, 2020, **152**, 224108.

36 A. D. Becke, A new mixing of Hartree--Fock and local density-functional theories, *J. Chem. Phys.*, 1993, **98**, 1372–1377.

37 T. H. Dunning Jr, Gaussian basis sets for use in correlated molecular calculations. I. The atoms boron through neon and hydrogen, *J. Chem. Phys.*, 1989, **90**, 1007–1023.

38 A. I. Krylov, Spin-flip equation-of-motion coupled-cluster electronic structure method for a description of excited states, bond breaking, diradicals, and triradicals, *Acc. Chem. Res.*, 2006, **39**, 83–91.

39 A. I. Krylov, Size-consistent wave functions for bond-breaking: The equation-of-motion spin-flip model, *Chem. Phys. Lett.*, 2001, **338**, 375–384.

40 M. Barone, V.; Cossi, Quantum calculation of molecular energies and energy gradients in solution by a conductor solvent model, *J. Phys. Chem. A*, 1998, **102**, 1995–2001.

41 F. Neese, F. Wennmohs, A. Hansen and U. Becker, Efficient, approximate and parallel Hartree--Fock and hybrid DFT calculations. A ‘chain-of-spheres’ algorithm for the

Author Manuscript

Hartree--Fock exchange, *Chem. Phys.*, 2009, **356**, 98–109.

42 A. D. Becke, Density-functional exchange-energy approximation with correct asymptotic behavior, *Phys. Rev. A*, 1988, **38**, 3098.

43 C. Reichardt, R. A. Vogt and C. E. Crespo-Hernández, On the origin of ultrafast nonradiative transitions in nitro-polycyclic aromatic hydrocarbons: Excited-state dynamics in 1-nitronaphthalene, *J. Chem. Phys.*, 2009, **131**, 0–15.

44 J. Snellenburg, S. Laptenok, R. Seger, K. Mullen, I. Van, J. Snellenburg, S. Laptenok, R. Seger, K. Mullen, I. V. S. G. A and R. Seger, Glotaran : A Java-based graphical user interface for the R package TIMP To cite this version : Glotaran : A Java -Based Graphical User Interface for, *J. Stat. Softw.*, 2012, **49**, 1–22.

45 J. R. Lakowicz, Principles of Fluorescence Spectroscopy 3rd Ed, 2006. New York, NY

46 J. R. Platt, Classification of spectra of cata-condensed hydrocarbons, *J. Chem. Phys.*, 1949, **17**, 484–495.

47 M. A. El-Sayed, The triplet state: its radiative and nonradiative properties, *Acc. Chem. Res.*, 1968, **1**, 8–16.

48 M. A. El-Sayed, Spin-orbit coupling and the radiationless processes in nitrogen heterocyclics, *J. Chem. Phys.*, 1963, **38**, 2834–2838.

49 S. Matsika, Electronic Structure Methods for the Description of Nonadiabatic Effects and Conical Intersections, *Chem. Rev.* 2021, **121**, 9407–9449.

50 L. V Slipchenko and A. I. Krylov, Singlet-triplet gaps in diradicals by the spin-flip approach: A benchmark study, *J. Chem. Phys.*, 2002, **117**, 4694–4708.

Author Manuscript

51 N. Minezawa and M. S. Gordon, Optimizing conical intersections by spin- flip density functional theory: application to ethylene, *J. Phys. Chem. A*, 2009, **113**, 12749–12753.

52 X. Zhang and J. M. Herbert, Analytic derivative couplings for spin-flip configuration interaction singles and spin-flip time-dependent density functional theory, *J. Chem. Phys.*, 2014, **141**, 64104.

53 L. M. F. Oliveira, D. Valverde, G. J. Costa and A. C. Borin, The copious photochemistry of 2, 6-diaminopurine: Luminescence, triplet population, and ground state recovery, *Photochem. Photobiol., 2023,* doi:10.1111/php.13833

Figure Captions

Scheme 1. Molecular structure of 2,6-diaminopurine derivatives investigated in this study. R is a methyl group in 9-methyl-2,6-diaminopurine, or a 2'-deoxyribose in 2,6-diaminopurine-2'-deoxyribonucleoside.

Figure 1. Molar absorption and emission spectra (λ_{exc} = 290 nm) of 9Me2,6DAP (blue) and 26DAP-d (magenta) in a) MeCN and b) phosphate buffer at pH 7.4. Bottom x-axis in nm and top x-axis in cm^{-1}. The E_{00} energy corresponding to the point of overlap between the two spectra is highlighted in the figure. Profile of excitation laser pulses used in the transient absorption measurements is shown in purple.

Figure 2. a) Representative optimized geometries of relevant points of the potential energy surfaces of 9Me2,6DAP at the B3LYP/CPCM/cc-pVDZ level of theory in MeCN. The geometry

of the $S_1(\pi\pi^*\ L_a)$ minimum was optimized using LR-TD-DFT and the minimum-energy crossing points between the $S_1(\pi\pi^*\ L_a)$ and the ground-state were optimized with SF-TD-DFT. b) Main (0.82) electronic transition of the lowest-energy excited single state $S_1(\pi\pi^*\ L_a)$ at the TD-BP86/CPCM/def2-TZVPD// B3LYP/CPCM/cc-pVDZ level of theory in MeCN.

Figure 3. Ground and the $S_1(\pi\pi^*\ L_a)$ states potential energy profiles along the C2-puckering and C6-puckering reaction coordinates for 9Me2,6DAP at the TD-BP86/CPCM/def2-TZVP//TD-B3LYP/CPCM/cc-pVDZ level of theory in MeCN. The energy barrier to access the conical intersections are shown as ΔE on the figure. See Figure 3 in ref. [15] for analogous the potential energy profiles for N9H tautomer of 2,6DAP in water at the same level of theory.

Figure 4. Transient absorption spectra of 9Me2,6DAP in MeCN upon excitation with 290 nm. The x-axis denotes the wavelength on a linear scale and the y-axis denotes the delay times in a linear-log scale. The break on the y-axis represents when the scale changes from linear to logarithmic scale. (Right) Representative decay traces at 390, 474 and 665 nm probe wavelengths with best fits obtained using a two-component sequential kinetic model. (Bottom) Two dimensional transient spectral evolution covering the time delays from -0.80 ps to 85 ps. The break on the x-axis is masking the scattering of the pump beam overtone reaching the detector.

Figure 5. Transient absorption spectra of 2,6DAP-d in MeCN upon excitation with 290 nm. The x-axis denotes the wavelength on a linear scale and the y-axis denotes the time delays in a linear-log scale. The break on the y-axis represents when the scale changes from linear to logarithmic scale. (Right) Representative decay traces at the 390, 474 and 665 nm probe wavelengths and best fits using a two-component sequential kinetic model. (Bottom) Two dimensional transient spectral evolution covering the time delays from -0.96 ps to 89 ps. The break on the x-axis is marking the scattering of the pump beam reaching the detector.

Author Manuscript

Figure 6. Transient absorption spectra of 9Me2,6DAP in phosphate buffer at pH 7.4 upon excitation with 290 nm. The x-axis denotes the wavelength on a linear scale and the y-axis denotes the delay times in a linear-log scale. The break on the y-axis represents when the scale changes from linear to logarithmic scale. (Right) Representative decay traces at 390, 474 and 665 nm probe wavelengths with best fits obtained using a two-component sequential kinetic model. (Bottom) Two dimensional transient spectral evolution covering the time delays from -1.3 ps to 507 ps. The break on the x-axis is masking the scattering of the pump beam overtone reaching the detector.

Figure 7. Transient absorption spectra of 2,6DAP-d in phosphate buffer at pH 7.4 upon excitation with 290 nm. The x-axis denotes the wavelength on a linear scale and the y-axis denotes the time delays in a linear-log scale. The break on the y-axis represents when the scale changes from linear to logarithmic scale. (Right) Representative decay traces at the 390, 474 and 665 nm probe wavelengths and best fits using a two-component sequential kinetic model. (Bottom) Two dimensional transient spectral evolution covering the time delays from -1.36 ps to 1059 ps. The break on the x-axis is marking the scattering of the pump beam reaching the detector.

Scheme 2. Proposed general electronic relaxation mechanism for 9Me2,6DAP and 2,6DAP-d in MeCN and in phosphate buffer solution at pH 7.4 according to the experimental and theoretical results reported in this study.

Author Manuscript

Table 1. Steady-state photophysical properties of 9Me2,6DAP and 2,6DAP-d.

	λ_{abs} (nm)	ε ($\times 10^3$ M^{-1} cm^{-1})	λ_{em} (nm)	Φ_{FL}
9Me2,6DAP[a]	280, 257, 215	9.5, 7.4, 2.6	352	0.0042 ± 0.0001
9Me2,6DAP[b]	280, 257, 217	9.4, 8.0, 2.8	335	0.0020 ± 0.0001
2,6DAP-d[a]	280, 256, 215	9.6, 8.6, 2.3	352	0.0058 ± 0.0008
2,6DAP-d[b]	280, 256, 217	9.1, 8.2, 2.4	335	0.0025 ± 0.0001

a. Aqueous phosphate buffer at pH 7.4 solution

b. MeCN solution

Table 2. Vertical excitation energies (in eV) for 9Me2,6DAP in MeCN calculated at the TD-BP86/CPCM/def2-TZVPD level of theory together with those reported previously for the N9H tautomer of 2,6DAP in water.[15] Energy values in wavelengths are also shown in brackets and oscillator strengths are shown in parentheses.

State	9Me2,6DAP in MeCN	2,6DAP in water[a]
$S_1(\pi\pi^*\ L_a)$	4.33 [286] (f = 0.17)	4.46 [278] (f = 0.20)
$T_1(\pi\pi^*)$	3.34 [371]	3.41 [364]
$T_2(\pi\pi^*)$	4.13 [300]	4.20 [295]

a. Reported in ref. [15]. Note that the vertical excitation energies reproduced herein from ref. [15] were performed for geometries optimized in vacuum.

Author Manuscript

Table 3. Lifetimes extracted from global and target analyses of the femtosecond transient absorption data of 9Me2,6DAP and 2,6DAP-d in MeCN and phosphate buffer at pH 7.4 upon excitation with 290 nm.

Compound	τ_1 (ps)	τ_2 (ps)
9Me2,6DAP (MeCN)	0.5 ± 0.1	20 ± 1
2,6DAP-d (MeCN)	0.5 ± 0.2	30 ± 1
9Me2,6DAP (pH 7.4)	1.1 ± 0.3	53 ± 3
2,6DAP-d (pH 7.4)	1.1 ± 0.3	74 ± 5

Author Manuscript

Author Manuscript

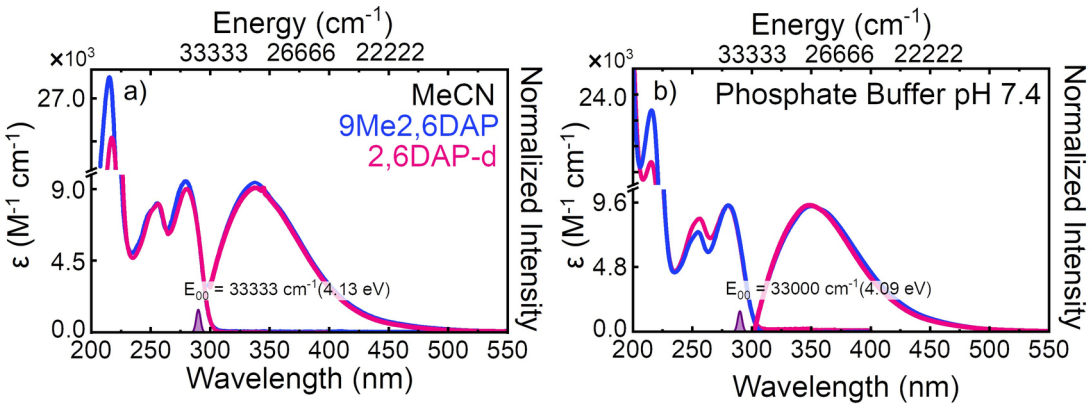


Figure1_600dpi.jpg

Author Manuscript

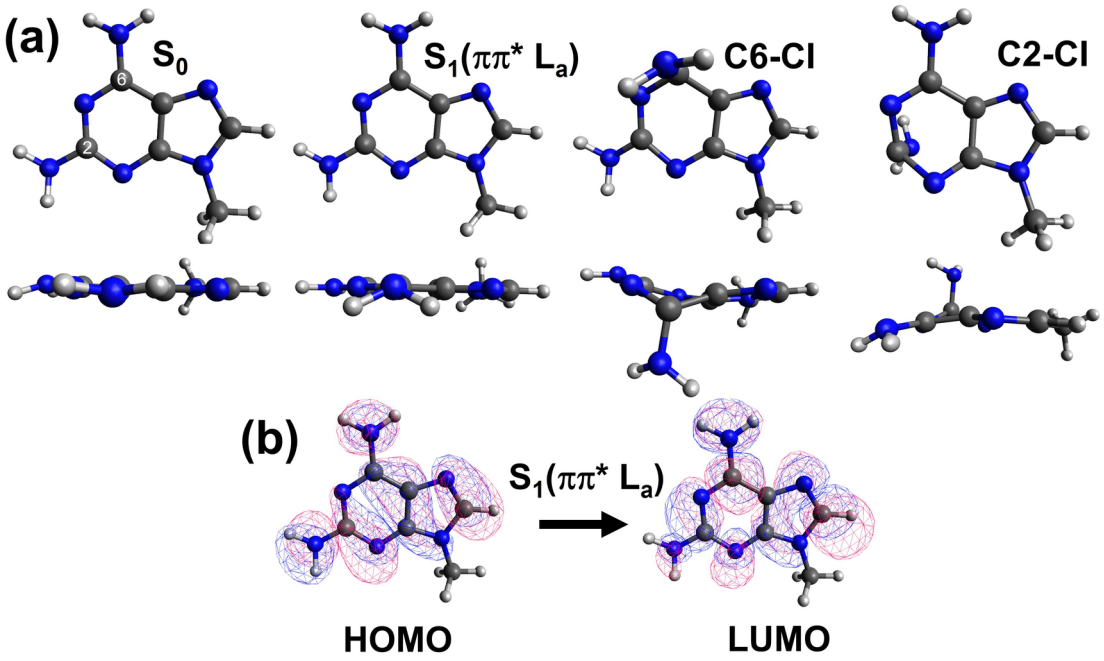


Figure2_600dpi.jpg

Author Manuscript

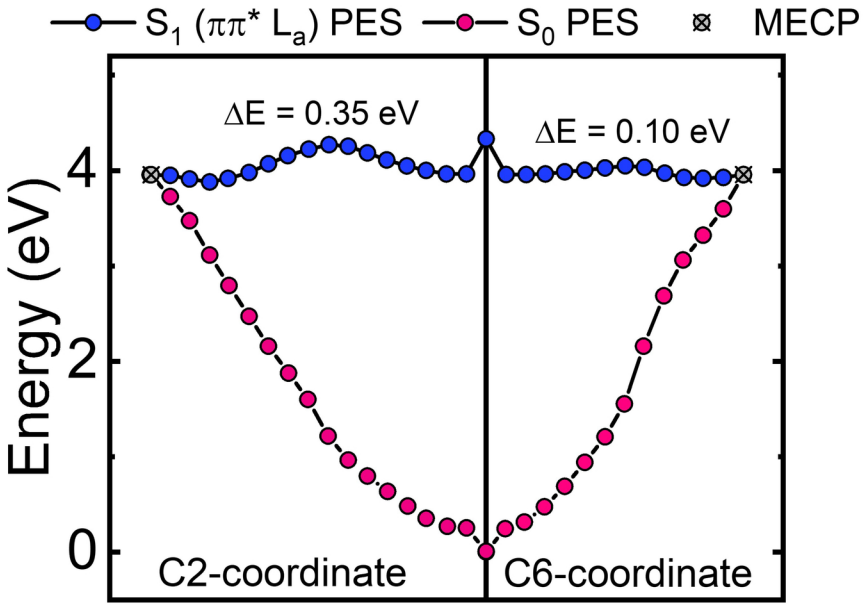


Figure3_600dpi.jpg

Author Manuscript

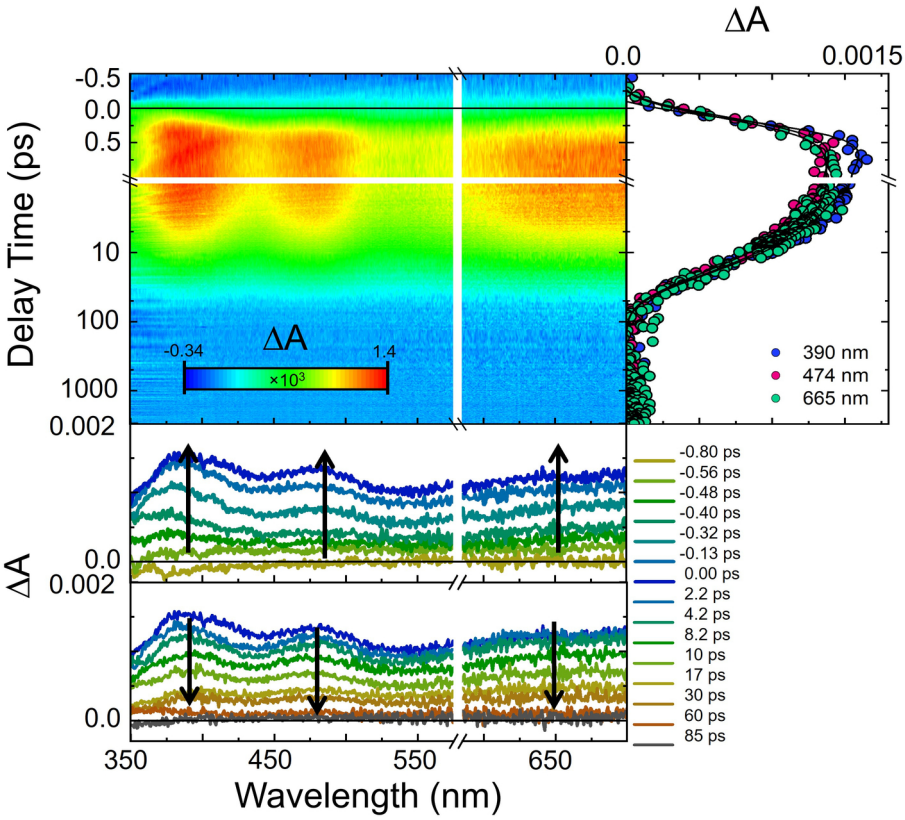


Figure4_600dpi.jpg

Author Manuscript

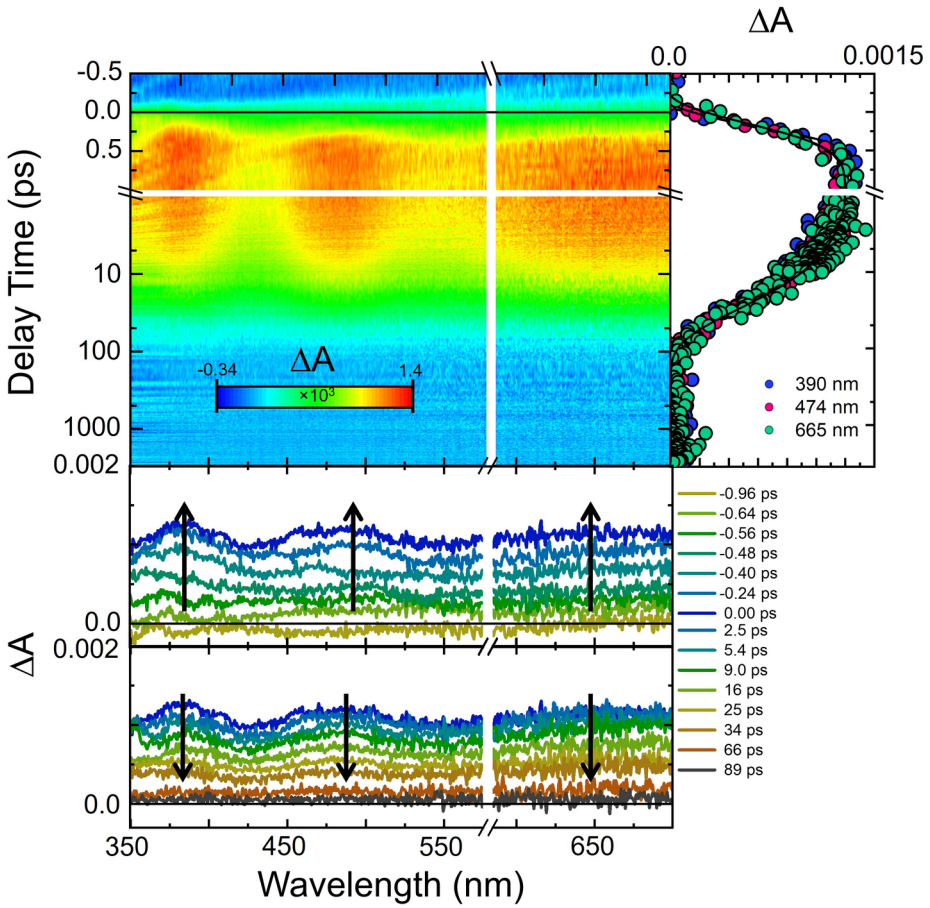


Figure5_600dpi.jpg

Author Manuscript

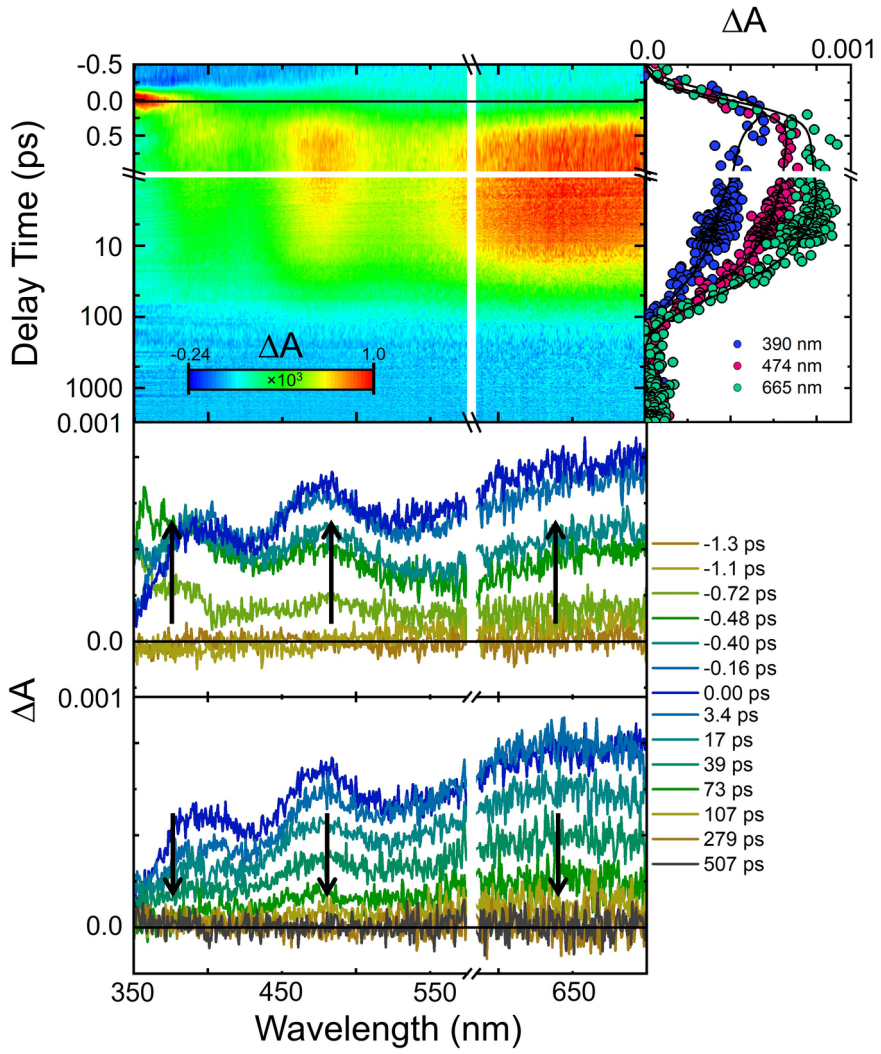


Figure6_600dpi.jpg

Author Manuscript

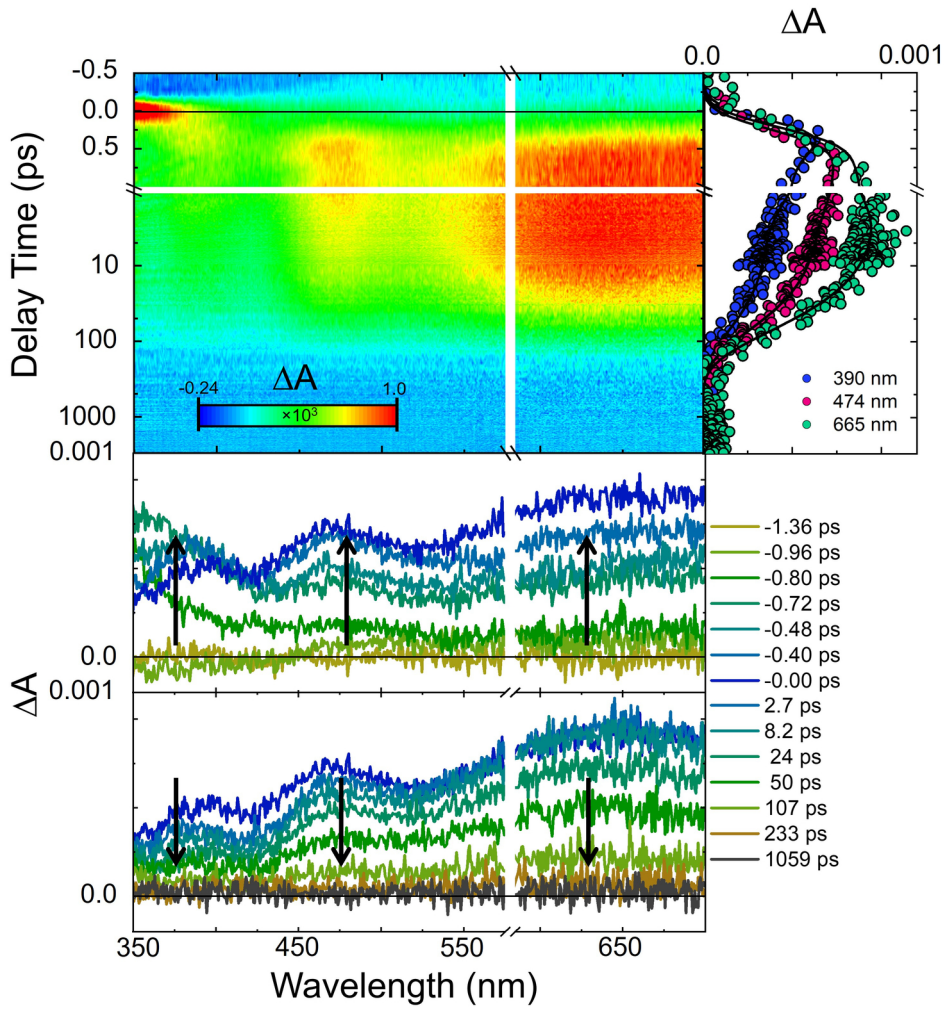
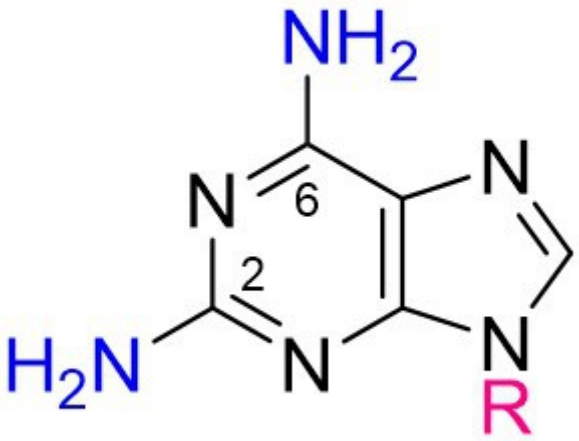


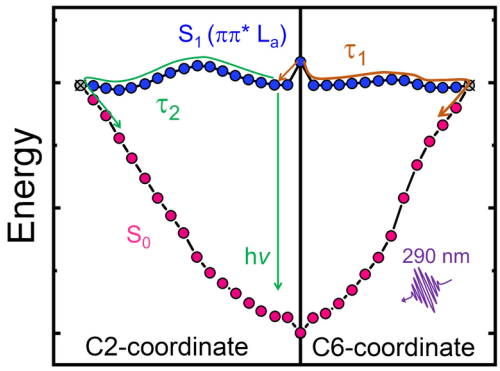
Figure7_600dpi.jpg

Author Manuscript



Scheme1__600dpi.jpg

Author Manuscript



Scheme2_600dpi.jpg